

# Automatic Anterior Chamber Angle Assessment Of Ultrasound Images For Glaucoma Detection

Sanskriti Naik<sup>1</sup>, Rini Rai<sup>2</sup>, Nimisha Sankhe<sup>3</sup>, P. V. Kasambe<sup>4</sup>

<sup>1</sup>(Department of Electronics Engineering  
Sardar Patel Institute of Technology, Mumbai, Maharashtra, India

<sup>2</sup>(Department of Electronics Engineering  
Sardar Patel Institute of Technology, Mumbai, Maharashtra, India

<sup>3</sup>(Department of Electronics Engineering  
Sardar Patel Institute of Technology, Mumbai, Maharashtra, India

<sup>4</sup>(Department of Electronics Engineering  
Sardar Patel Institute of Technology, Mumbai, Maharashtra, India

## Abstract

*Glaucoma refers to a group of ocular diseases that usually have few or no initial symptoms and may cause characteristic progressive changes in the optic nerve head, visual field loss or both. Image processing techniques for the ultrasound images of the eye can be used to extract critical parameters pertaining to the structural changes in the anterior chamber of the eye which can help in glaucoma detection. We propose an algorithm to automatically detect the anterior chamber region and measure one such critical parameter, the Trabecular Iris Angle. Among the many challenges encountered in implementing the proposed algorithm, a significant one was the extraction of the ciliary body region amidst ultrasound speckle noise; this has been tackled using a combination of two filters, namely, adaptive Wiener filter and Laplacian of Gaussian filter. Also, a graphical user interface was developed for simple and convenient user accessibility.*

## 1. Introduction

The glaucomas are a diverse group of eye conditions sharing the common features of progressive optic neuropathy or occludable drainage angles in the anterior chamber [1]. Glaucoma is second only to cataract as a leading cause of blindness worldwide [2]

and is the leading cause of irreversible visual loss. As 50% or more of those individuals with glaucoma are unaware of their diagnosis, more effort is needed to effectively screen high-risk groups and to educate society about the preventability and consequences of glaucoma [3].

Primary open angle glaucoma is a degenerative disorder of the eye, where the intraocular pressure and other currently unknown factors contribute to a characteristic acquired atrophy of the optic nerve [4]. Primary angle closure (PAC) is an anatomical disorder of the anterior segment of the eye characterized by permanent closure of part of the filtration angle as a result of previous iris apposition to the trabecular meshwork. The subsequent rise in intraocular pressure can cause optic nerve damage and is defined as primary angle closure glaucoma (PACG) [5].

By the year 2020, it is estimated that there will be almost 80 million people in the world with open-angle glaucoma and angle-closure glaucoma (ACG). In the year 2010, it was estimated that ACG will account for 26% of glaucoma worldwide, with a mean prevalence of 0.69%. Due to greater longevity of women and the higher prevalence of ACG in women, women are expected to comprise 70% of individuals with ACG [3]. Hence, the screening and diagnosis of ACG is very important. If untreated, it leads to higher intraocular pressure, permanent nerve damage, and blindness.

Reduction of the intraocular pressure through treatment consisting of medication or surgery can effectively stop the progression of the nerve fibre layer loss. Hence, the diagnosis of glaucoma at an earlier stage is very crucial to its treatment.

Glaucoma does not exhibit any particular set of physical causes and it is asymptomatic in the early stage. It is often only recognized when the disease is quite advanced and vision is lost. Hence, the main focus in glaucoma diagnosis is the detection of changes in the visual functioning of the eye in the early stages of the disease, so that vision can be protected and preserved through medical treatment.

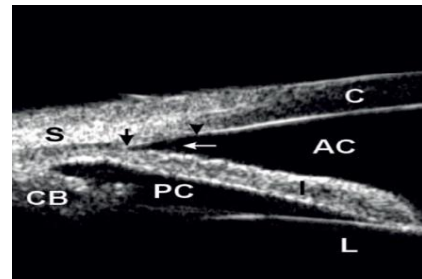
Examining the anterior chamber angle is an indispensable component in the ophthalmic assessment of any individual who is diagnosed with or suspected of having glaucoma. The anterior chamber angle is the actual anatomical angle created by the root of the iris and the peripheral corneal vault. The structures involved in the outflow of the aqueous humour lie within this chamber [6]. Anterior chamber angle assessment is used for the detection of ACG and is essential in deciding whether or not to perform laser iridotomy, which is a surgical procedure to re-establish aqueous flow between the posterior and anterior chamber [7]. The early detection of anatomically narrow angles is important, and the subsequent prevention of visual loss from PACG depends on an accurate assessment of the anterior chamber angle (ACA). Various biomedical methods have been used for the detection of glaucoma by visualizing and measuring the ACA, popular among them being Gonioscopy, Ultrasound Bio-Microscopy (UBM) and Anterior Segment – Optical Coherence Tomography (AS -OCT)[5].

Gonioscopy makes it possible to directly visualize the anterior chamber angle under a slit lamp, but the examination is essentially subjective and qualitative. It has given way to modern clinical imaging modalities like UBM and AS-OCT. UBM is ideally suited to the study of ACG because of its ability to simultaneously display the ciliary body, posterior chamber, iris-lens relationships and angle structures [8]. UBM provides objective, high-resolution images of anterior segment anatomy, with tissue resolution of approximately  $50\mu\text{m}$  and penetration depth of 5 mm, providing a useful diagnostic tool for narrow angles and other anterior chamber pathologies [9].

In the anterior chamber region, the only landmark which can be distinguished consistently is the scleral spur [10]. The scleral spur is a protrusion of the sclera anchoring the trabecular meshwork anteriorly and the longitudinal muscle of the ciliary body posteriorly. It represents an anatomical landmark for the trabecular

meshwork which is located approximately 250 to 500  $\mu\text{m}$  anterior to the scleral spur along the angle wall. Due to the different tissue reflectivity between the sclera and cornea, the scleral spur can be visualized in UBM as a distinct anatomical landmark for the measurement of the ACA [9], [11], [12].

In a UBM image, the scleral spur can be seen as the innermost point of the line separating the ciliary body and the sclera at its point of contact with the anterior chamber. Thus, the essential structures for the diagnosis of angle-closure glaucoma are clearly visible in a UBM image [11]. Fig. 1 shows the angle structures visible in a UBM ocular image.



**Figure 1.** Ultrasound Bio-microscopy image showing normal angle structures. S: sclera; CB: ciliary body, PC: posterior chamber, AC: anterior chamber, L: lens, C: cornea. Dark arrows delineate the trabecular meshwork from the scleral spur towards Schwalbe's line while the white arrow signals points towards an open angle.

The various angle structures in the ultrasound images of the eye are manually analysed by a technician. A trained expert determines the anatomical features of interest and measures the relevant clinical parameters. The parameters are measured on the UBM monitor, allowing determination of a point-to-point distance or an angle composed of two straight lines; this method removes the previous measurements from the screen, making it difficult to perform multiple-step measurements [10]. Hence we were motivated to develop an algorithm that will automatically analyse the ultrasound images of the eye and extract the required parameters. We anticipate that this algorithm will reduce the processing time currently taken by the technician to analyse the images. Also since the same algorithm will be used for all the images, any discrepancy arising due to the difference in the expertise of the technician is removed.

In this paper, we describe an algorithm to assess the anterior chamber angle based on the detection of the ciliary body and the scleral spur. The details are presented in Section II. Experiments to test the performance of our algorithm are described and results are discussed in Section III. We conclude and suggest some future work in Section IV.

## 2. Algorithm Design

UBM offers tremendous insight into the anterior chamber angle configuration and allows for detailed imaging of the ciliary body and the posterior chamber [13]. The method proposed by us involves the automatic extraction of two vital structures, namely, the anterior chamber and the ciliary body, followed by the determination of the apex and the scleral spur coordinates. These are the clinically relevant features which assist in the computation of the Trabecular Iris Angle (TIA).

Our method for determining the Trabecular Iris Angle involves the following steps:

1. Ultrasound image enhancement,
2. Edge detection and segmentation of anterior chamber,
3. Ciliary body segmentation, and
4. Calculation of the TIA.

The flowchart of the algorithm is shown in Fig.4 and the details of the procedure are explained in the following subsections.

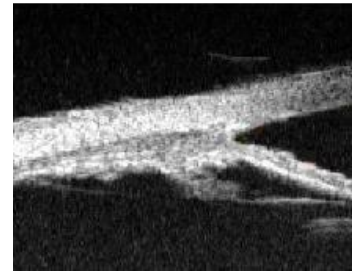
### 2.1. STEP 1: Ultrasound image enhancement

The objective of this step is to refine the ultrasound image to make it fit for effective anterior chamber segmentation.

The image in Fig. 2 is the original UBM ocular image to which the algorithm has been applied. Ultrasound image enhancement is done using the following steps:

**2.1.1. Thresholding.** Thresholding helps in highlighting the object of interest by selecting an appropriate value of threshold. Individual pixels in the image are marked as 'object' pixels if their value is greater than the threshold value and as 'background' pixels otherwise. The object pixel is given a value of '1' while the background pixel is given a value of '0'. After thresholding, the object of interest (i.e. the eye) appears white and is highlighted whereas other pixels in the image appear black.

**2.1.2. 2D Median filtering.** Median filtering is necessary to perform a high degree of noise reduction in the image before performing higher-level processing steps, such as edge detection. The 2D median filter used in this algorithm considers each pixel in the image and looks at its nearby neighbours to decide whether or not it is a representative of its surroundings. It reduces salt and pepper noise in the ultrasound image.



**Figure 2.**One of the original sample UBM images taken for testing, before processing.

**2.1.3. Erosion.** Erosion removes small spurious, bright spots inside the anterior chamber region. This is a pre requisite to give a well-defined angle. A flat, linear structuring element has been used for this purpose.

**2.1.4. Hole-filling.** Small openings (holes) in the trabecular meshwork and the iris are been detected and filled to produce a smooth, flawless image for efficient and effective anterior chamber classification and segmentation. Fig. 3 shows the resultant image of the hole-filling operation.



**Figure 3.**Result of the Image enhancement operation.

### 2.2. STEP 2: Edge detection and segmentation of anterior chamber

The objective of this step is to extract the anterior chamber region and locate the co-ordinates of the apex.

**2.2.1. Edge detection.** Edge detection is a fundamental of low-level image processing and good edges are necessary for accurate segmentation. The 'Laplacian of Gaussian' filter has been used for edge detection.

**2.2.2. Segmentation of anterior chamber.** The segmentation process involves the following sub steps:

#### a) Classification of regions

Every connected region of the edge-detected image is classified according to its area (total number of pixels characterizing the closed region) and labelled.

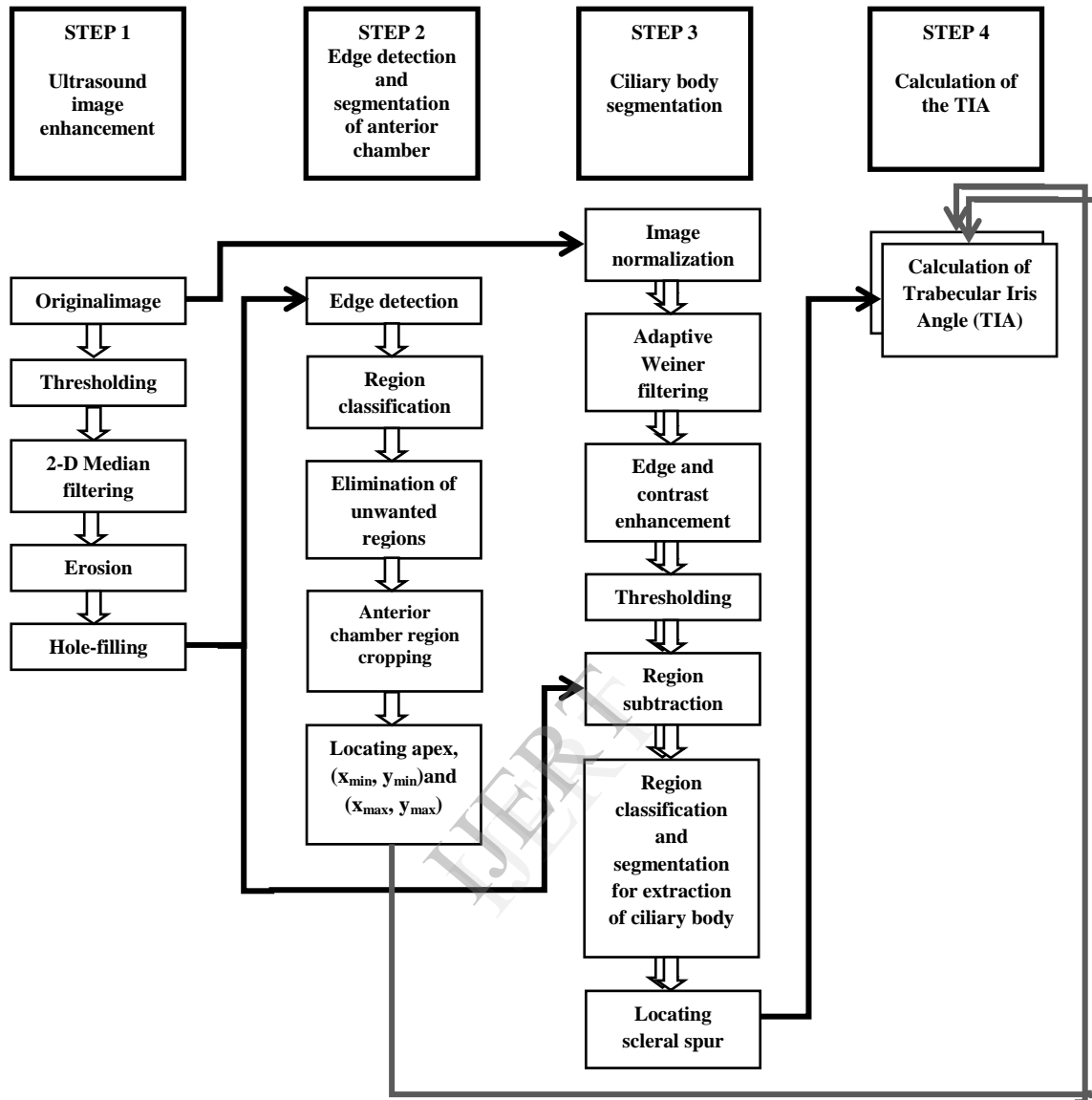


Figure 4. Flowchart of the proposed algorithm.

**b) Elimination of unwanted regions**

The area of each of the classified regions is compared with a standard pixel area and regions having an area greater than the selected standard pixel area are eliminated to narrow down the choices to a few regions including the anterior chamber, which is the primary region of interest.

**c) Cropping the anterior chamber region**

The other smaller regions excluding the anterior chamber that remain after the previous operation are eliminated by further area-based classification.

Fig. 5 shows the angle contained in the cropped anterior chamber region obtained at the end of this step.



Figure 5. The cropped anterior chamber region.

**2.2.3. Locating the co-ordinates of the apex.** The apex co-ordinates are found by locating a white pixel which is most to the left of the anterior chamber region. Also, the rightmost end-points,  $(x_{min}, y_{min})$  and  $(x_{max}, y_{max})$ , of the anterior chamber region are detected which are required for further calculations.

**2.3. STEP 3: Extraction of the ciliary body**

The objective of this step is to extract the ciliary body region which is essential for locating the scleral spur.

**2.3.1. Image normalization**

Normalization changes the range of pixel intensity values and enhances the texture of interest. It is applied on the ultrasound image using equation 1.

$$I'(x, y) = (I(x, y) - tL) \left( \frac{255}{tH - tL} \right) \dots \dots \dots (1)$$

where  $I(x, y)$  and  $I'(x, y)$  are the input and output pixels respectively.

Threshold values are calculated such that  $tL$  and  $tH$  are 15% and 85% of the maximum pixel value in the image, respectively. The normalized image shows better contrast and delineation around the ciliary body region.

**2.3.2. Adaptive Wiener filtering.** The adaptive Wiener filter performs low-pass filtering on the image based on statistics estimated from the local neighbourhood of each pixel. A 9x9 pixel neighbourhood is chosen to adaptively reduce high frequencies in the image prior to fine enhancement.

**2.3.3. Edge and contrast enhancement.** Laplacian of Gaussian (LoG) filter is used for non-linear edge and contrast enhancement. The main advantage of LoG filter is less number of arithmetic computations required, which leads to faster processing. The first stage of filtering applies a Gaussian smoothing operator to blur the image and remove detail and noise. Further, the Laplacian is applied, which highlights regions of rapid intensity change. The enhanced image contains the ciliary body which is required for locating the scleral spur.

**2.3.4. Thresholding.** The enhanced image is thresholded using the process described in section 2.1.1.

**2.3.5. Region subtraction.** The thresholded image is subtracted from the hole-filled image obtained in step 1. This eliminates all the large regions in the image and keeps only the details of interest, which includes the ciliary body.

**2.3.6. Region classification and segmentation.** For the segmentation of the ciliary body, each closed region obtained is classified according to its area and labelled. Then, only the region having an area greater than an appropriately chosen standard pixel area is retained. In Fig. 6 the extracted ciliary body region is shown.

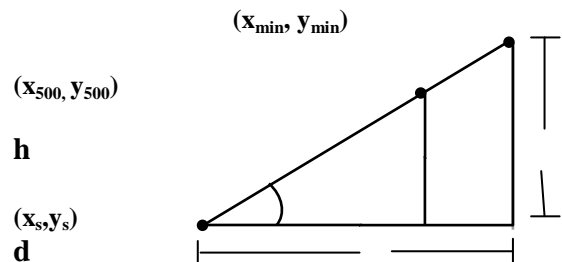


**Figure 6.** The extracted ciliary body region.

**2.3.7. Locating the co-ordinates of the scleral spur.** The scleral spur is the key to analysing the angle pathology. It lies at the most posterior end of the trabecular meshwork on the posterior corneoscleral-aqueous interface. It can be found by locating the topmost point of the ciliary body to the right.

**2.4. STEP 4: Calculation of the TIA**

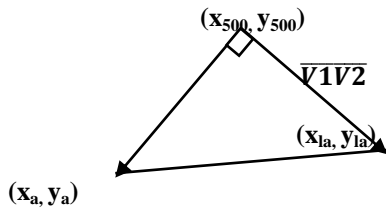
The calculation of the TIA requires the co-ordinates,  $(x_{500}, y_{500})$ , of a point 500µm away from the scleral spur along the upper half of the anterior chamber which can be obtained from the scleral spur co-ordinates and the topmost end point  $(x_{min}, y_{min})$ . The obtained co-ordinates,  $(x_{500}, y_{500})$ , provide data for defining the upper and lower contours. Fig.7 shows the co-ordinates,  $(x_{500}, y_{500})$ , of a point on the upper contour, along the line joining the scleral spur and the point  $(x_{min}, y_{min})$ .



**Figure 7.** Obtaining the co-ordinates  $(x_{500}, y_{500})$ .

The orthogonal projection co-ordinates,  $(x_{la}, y_{la})$ , along the lower iris trace can be obtained by taking the dot product between the vectors  $\vec{V1}$  and  $\vec{V2}$  as shown in Fig. 8.

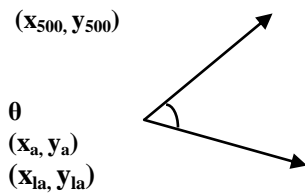




**Figure 8.** Finding the orthogonal projection co-ordinates.

If the apex is to the left of the 500 μm co-ordinate then, the angle, in radians, is calculated as:

$$\theta = \cos^{-1} \left[ \frac{(\overline{V1} \cdot \overline{V3})}{(|\overline{V1}| * |\overline{V3}|)} \right] \dots\dots\dots (2)$$



**Figure 9.** Computation of the TIA.

If the apex lies to the right of the 500μm co-ordinate, then the angle is 0 degrees. Fig. 9 shows the TIA named as θ.

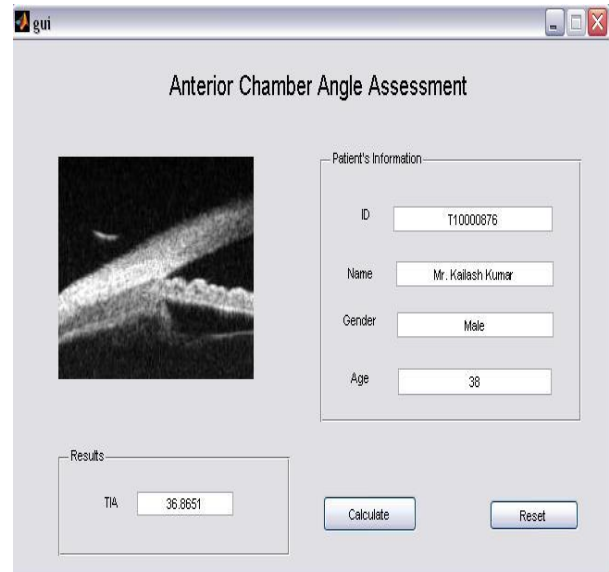
**3. Results**

We obtained 10 UBM ocular images from UBM Institute, Mumbai for testing and verifying our algorithm. The images obtained from the UBM machine were analysed by the technician to obtain the required features manually. The TIA is calculated using callipers and manually plotting the points of interest on the image by using a software called UBM Pro provided by Sonomed, Inc.

The software programs for our algorithm were written in MATLAB 7.10 (R2010a). The images were processed on a 2600 MHz Quad core AMD Athlon II X4 620 Processor. The algorithm was used to process the obtained images, with an execution time of 3.3 seconds for one image.

We analysed the obtained UBM images and determined whether our algorithm was able to faithfully extract the required clinical parameters. An accuracy of 91.67% was noted according to the results of the algorithm. The accuracy was affected as one of the images was of poor contrast which led to improper segmentation of ciliary body.

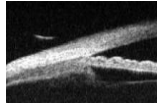
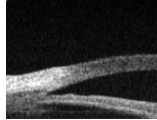

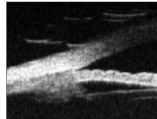
The GUI for the discussed algorithm is shown in the figure 10.



**Figure 10.** GUI for the proposed algorithm.

The results obtained on a few images have been presented in Table 1.

**Table1**  
Comparison of the angles obtained through manual processing and the proposed algorithm

Sr. no.	Image	Manually computed angle (Degrees)	Angle (Degrees)
1		33.57	36.8651
2		23.62	26.56
3		67.9	63.4267
4		19.6	21.798

#### 4. Conclusion

The aim of this paper is to propose an algorithm for automatic identification of the clinical parameters of ultrasound images of the eye. The opening angle is calculated. These values help the physician in the analysis of the patient's glaucoma. The observations from the algorithm are very similar to that obtained by the technician, with very small error margin. The primary difficulties encountered in implementing this algorithm were noise and poor contrast. These mainly affected the calculation of the scleral spur. The main advantage of the proposed algorithm is the reduction in the time required to calculate the trabecular iris angle. This will help in faster diagnosis and, hence, better treatment.

This work can be further expanded by interfacing the GUI with the hardware for obtaining the UBM ocular images.

#### 5. Acknowledgement

The authors gratefully acknowledge Dr. Deepak Bhatt of UBM Institute, Mumbai for providing us with images for our study and demonstrating the manual processing of the UBM ocular images. The authors would also thank the Electronics Engineering department at Sardar Patel Institute of Technology for providing computing support in the VLSI and Embedded Systems laboratory.

#### 6. References

- [1] J. D. Stein and P. L. Lee, "Screening for Glaucoma," in *Ophthalmology*, 2<sup>nd</sup> ed., USA: Mosby Elsevier, 2004, pp. 1102.
- [2] S. Resnikoff, D. Pascolini, D. Etya'ale, I. Kocur, R. Pararajasegaram, G. Pokharel and S. Mariotti, "Global data on visual impairment in the year 2002," *Bulletin of the World Health Organization*, 2004; 82:844-851.
- [3] A. Giangiacomo, A. Coleman, "The Epidemiology of Glaucoma," in *Essentials in Ophthalmology: Glaucoma*, F. Grehn and R. Stamper, Ed. Springer, 2009, pp. 19.
- [4] J. Tsai and M. Forbes, "Introduction: Primary Open-Angle Glaucoma," in *Medical Management of Glaucoma*, 3<sup>rd</sup> ed., USA, Professional Communications, Inc., 2009, pp. 11.
- [5] A. Fea, L. Bertaina, G. Consolandi, D. Damato, U. Lorenzi and F. Grignolo, "Angle Closure Glaucoma: Pathogenesis and Evaluation. A Review," *J Clinic Experiment Ophthalmol* S4:005, 2012.
- [6] C. Campa, L. Pierro, P. Bettin and F. Bandello, "Anterior Chamber Angle Assessment Techniques," in *Glaucoma - Basic and Clinical Concepts*, S. Rumelt, Ed. InTech, 2011.
- [7] D. Gupta, "Glaucoma: Diagnosis and Management," Lippincott Williams and Wilkins, Philadelphia, 2005, pp. 131.
- [8] R. Ritch, J. Liebmann and C. Tello, "A Construct for Understanding Angle-Closure Glaucoma," *Ophthalmology Clinics of North America*, vol. 8, no. 2, pp. 281, June 1995.
- [9] S. Dorairaj, J. Tsai, and T. Grippo, "Changing Trends of Imaging in Angle Closure Evaluation," *ISRN Ophthalmology*, vol.2012, Article ID 597124, 2012.
- [10] H. Ishikawa and J. Schuman, "Anterior Segment Imaging: Ultrasound biomicroscopy," *Ophthalmology Clinics of North America*, 17(1): 7-20, March 2004.
- [11] C. Pavlin, K. Harasiewicz, and F. Foster, "Ultrasound biomicroscopy of anterior segment structures in normal and glaucomatous eyes," *American Journal of Ophthalmology*, vol. 113, no. 4, pp. 381-389, 1992.
- [12] C. Pavlin and F. S. Foster, "Ultrasound biomicroscopy in glaucoma," *ActaOphthalmologicaSupplementum*, no. 204, pp. 7-9, 1992.
- [13] D. Friedman and M. He, "Anterior Chamber Angle Assessment Techniques," *Survey of Ophthalmology* vol. 53, no.3, May- June 2008, pp. 250-275.